frontiers in Materials

ORIGINAL RESEARCH
published: 01 February 2018
doi: 10.3389/fmats.2018.00003

Thin Bioactive Zn Substituted Hydroxyapatite Coating Deposited on Ultrafine-Grained Titanium Substrate: Structure Analysis

Konstantin A. Prosolov[1,2], Olga A. Belyavskaya[1], Uwe Muehle[3] and Yurii P. Sharkeev[1,2]*

[1] *Laboratory of Physics of Nanostructured Biocomposites, Institute of Strength Physics and Materials Science of SB RAS, Tomsk, Russia,* [2] *Department of Experimental Physics, National Research Tomsk Polytechnic University, Tomsk, Russia,* [3] *Fraunhofer Institute for Ceramic Technologies and Systems, Dresden, Germany*

Nanocrystalline Zn-substituted hydroxyapatite coatings were deposited by radiofrequency magnetron sputtering on the surface of ultrafine-grained titanium substrates. Cross-section transmission electron microscopy provided information about the morphology and texture of the thin film while in-column energy dispersive X-ray analysis confirmed the presence of Zn in the coating. The Zn-substituted hydroxyapatite coating was formed by an equiaxed polycrystalline grain structure. Effect of substrate crystallinity on the structure of deposited coating is discussed. An amorphous TiO_2 sublayer of 8-nm thickness was detected in the interface between the polycrystalline coating and the Ti substrate. Its appearance in the amorphous state is attributed to prior to deposition etching of the substrate and subsequent condensation of oxygen-containing species sputtered from the target. This layer contributes to the high coating-to-substrate adhesion. The major P–O vibrational modes of high intensity were detected by Raman spectroscopy. The Zn-substituted hydroxyapatite could be a material of choice when antibacterial osteoconductive coating with a possibility of withstanding mechanical stress during implantation and service is needed.

Keywords: antibacterial activity, hydroxyapatite, structure analysis, thin coatings, plasma coatings, biocompatibility, ultrafine-grained structure, high-resolution TEM

OPEN ACCESS

Edited by:
Alina Vladescu, National Institute for Research and Development in Optoelectronics, Romania

Reviewed by:
Miroslaw Bramowicz, University of Warmia and Mazury in Olsztyn, Poland
Catalin Pruncu, University of Birmingham, United Kingdom

****Correspondence:***
Konstantin A. Prosolov
konstprosolov@gmail.com

Specialty section:
This article was submitted to Thin Solid Films, a section of the journal Frontiers in Materials

Received: *08 December 2017*
Accepted: *10 January 2018*
Published: *01 February 2018*

Citation:
Prosolov KA, Belyavskaya OA, Muehle U and Sharkeev YP (2018) Thin Bioactive Zn Substituted Hydroxyapatite Coating Deposited on Ultrafine-Grained Titanium Substrate: Structure Analysis. Front. Mater. 5:3. doi: 10.3389/fmats.2018.00003

INTRODUCTION

With a population aging, increasing number of surgical procedures involving prosthesis implantation takes place. The current approach of regenerative medicine involves tissue engineering and implants with tailored properties which should be manufactured in accordance with the patient's clinical case (Pacelli et al., 2016). Implants made of titanium (Ti) or its alloys do not provide the required bioactivity. Therefore, metallic implants with various calcium phosphate coatings are gaining more and more attention (Gross et al., 2010; Rau et al., 2015).

Herewith, substituted hydroxyapatites (HA) are one of the most promising materials. Divalent cations, such as Zn, Fe, Cu, Mg, Ni, Cr, Mn, Co, Sr, Pb, and Cd, and anions such as F^-, Cl^-, CO_3^{2-}, and VO_4^{3-} may substitute for Ca^{2+}, OH^-, and $(PO_4)^{3-}$ in the HA structure. Easiness of atomic doping or substitution in apatite reveals its potential to be used in various clinical cases starting from its use in bone fracture fixation or defect filler to antimicrobial activity (Šupová, 2015). In the case of biomaterials which are designed to be implanted, it is important to create an antimicrobial surface that will be resistant to the adhesion and spreading of unwanted pathogenic bacteria (Graziani et al.,

2016). Moreover, in case of bacterial biofilm formation, infection and septic instability of implants is a significant threat (Koo et al., 2017). There is always a risk of bacterial entry to the implantation site during surgery, which could be associated with non-sterility of the equipment or the fact that surgeries are performed in open air conditions (George et al., 2016). This problem is especially important for elderly people and patients with compromised immune systems (Albrektsson et al., 2016; Bartold et al., 2016).

There is an emerging number of studies with regard to substituted HA with antimicrobial properties. It has been shown that ions of Ag, Cu, and Zn play a crucial role in the prevention of bacterial adhesion and spreading (Chung et al., 2006). Cu and Zn ions in small quantities are vital for various metabolic processes in living organisms, while at a higher concentration they could potentially lead to toxic effects. Among those ions, Zn is gaining attention as a not only antibacterial element but as an agent which stimulates bone growth (Li et al., 2009). Since it is of major interest to develop a system that not only prevents pathogenic bacteria colonization but also promotes bone growth, Zn was chosen as a doping element in our case.

One of the requirements for a substrate material is its biocompatibility (Sharkeev et al., 2016). On the other hand, implantable devices should have significant mechanical strength, especially under the influence of dynamic loads (Podaropoulos et al., 2016). The high mechanical properties will ensure the durability of manufactured medical products. Clinical practice and many scientific reports show a high level of biocompatibility of commercially pure (CP) Ti (Sidambe, 2014). However, its mechanical characteristics can be improved by severe plastic deformation (SPD) (Toth and Gu, 2014). Interestingly, the proliferation of fibroblastic cells and stem cells on the surface of nanostructured Ti processed by SPD has been shown to be promoted by grain refinement (Valiev et al., 2016). Another group of researchers (Mora-Sanchez et al., 2016) confirms that significant grain refinement by SPD processing leads to an improvement in mechanical and functional properties. Therefore, ultrafine-grained (UFG) Ti is a good candidate for a base material of a future successful implant.

There is a wide variety of coating techniques which could be used for Ti substrate treatment. Methods such as sol-gel (Asri et al., 2016), chemical (Wen et al., 1998), micro arc oxidation (Sedelnikova et al., 2016; Sharkeev et al., 2017), and others. Among them, the method of radiofrequency (RF) magnetron sputtering stands out. There are two major features of RF magnetron sputtering that are advantageous. First, good adhesion between coating and substrate and, second, the availability of sputtering targets with different chemical compositions which determine the composition of the synthesized coating (Surmeneva et al., 2014). In addition, RF magnetron sputtering is a highly controlled and reproducible process. Coating properties, such as thickness, microstructure, and crystallinity as well as chemical composition of a coating can be precisely controlled and tailored according to the needs (Vladescu et al., 2016).

In the present paper, Zn doped HA (HA-Zn) coatings with a chemical composition of $Ca_{10-x}Zn_x(PO_4)_6(OH)_{2-x}$, $x = 0.4$ are deposited on UFG Ti substrate. The coatings were deposited by RF magnetron sputtering method. It is possible to find recent reports on the deposition of strontium and zinc Co-substituted HA coatings by Robinson et al. (2017). But to our knowledge, the studies with regard to Zn containing HA coatings, especially when deposited on UFG Ti are very limited in the scientific community. Therefore, we are introducing our research results with regard to the structure and deposition parameters of bioactive antibacterial thin HA-Zn coatings. The structure of the thin films was studied in cross-section Transmission Electron Microscopy (TEM). The TEM samples were prepared by means of Focused Ion Beam (FIB) milling in Electron Microscope (SEM) assuring a high quality of the lamella. The deposited coatings adhesion was evaluated by a scratch testing.

MATERIALS AND METHODS

A well-established method of SPD has been used to obtain the bulk Ti in UFG state. CP coarse-grain Ti (99.58 Ti, 0.12 O, 0.18 Fe, 0.07 C, 0.04 N, 0.01 H wt%) was used as an initial material. First, Ti billets underwent multiple uniaxial pressing in a press-mold at 10^{-3} to 10^{-2} s speed range with a stepwise temperature decrease from 750 to 350°C. Uniaxial pressing at a fixed temperature was gradually carried out along three deformation axes. Second, the plastic deformation was applied with rollers of grooved or flat shape at room temperature to produce further grain refinement and to reach the nanostructured state. The total value of rolling deformation was 90%. Then the rolled sticks and plates were subjected to prior-to-recrystallization annealing at 250°C (Sharkeev et al., 2009). After this, samples were cut in the shape of plates with sizes of the 10 mm × 10 mm × 1 mm in order to be used as substrates for the deposition. The samples were polished in series using silicon–carbide paper up to 1,200 grit. Prior to deposition, the samples were sonicated for 10 min consecutively in acetone, ethanol, and distilled deionized water. The metallography imaging of CP coarse-grain Ti was done using inverted Olympus GX microscope (Japan) with available magnification from 5× to 100× for both brightfield and polarizing observations. The structure investigation of Ti samples after SPD was performed in TEM JEM 2100 (JEOL, Japan) available at the Center for Collective Use of Scientific Equipment "Nanotekh" of ISPMS SB RAS.

The HA-Zn powder was prepared by mechanochemical synthesis. Calcium hydrogen phosphate, calcium oxide, and zinc oxide were used in the process. The precursor powders were placed in a planetary ball mill with three drums, each having a volume of 1,800 mL. The process of synthesis took 12 min at a room temperature. The phase composition of HA-Zn powder was confirmed by X-ray diffraction. The process of target manufacturing from the initial powder of HA-Zn is described in detail in our previous study (Prosolov et al., 2017). The temperature for a target sintering was set to 1,100°C for 1 h in a stepwise manner. As a result, the heating and cooling to sinter each target took up to a day and a half. Target sintering resulted in a disk-shaped ceramic plate with a diameter of 120 and 5 mm thickness.

A vacuum installation, with a planar magnetron, was operated at the frequency of 13.56 MHz in order to deposit the HA-Zn coatings on the UFG Ti substrates. Prior to deposition, a closed electron drift ion source (TPU, Tomsk, Russia) was used for

substrate cleaning and etching of the natural TiO_2 layer. The surface activation was done for 15 min with an ion source parameter of 1.5–3.0 keV, a current of 10–30 mA, and a chamber pressure of 1 Pa. The coatings were prepared by magnetron sputtering at RF-power level of 250 W in an Ar atmosphere. The deposition time was 3 h, and the target-to-substrate distance was 60 mm. The substrate temperature measured by thermocouple did not exceed 80°C. The substrates were placed in the region of the target erosion zone. During the coating deposition, the working pressure in the vacuum chamber was 0.7 Pa. The average thickness of the coatings, as measured by a Calotest (CSEM Instruments) was 470 ± 15 nm.

Before FIB sample preparation UFG Ti plates with HA-Zn coating were cut with a Leco VC-50 Precision Diamond Cutter (USA). Subsequently, the sample surface was coated with a conductive layer of Au\Pd using a Polaron E5100 SEM coating unit, applying a current of 20 μA at a chamber pressure of 0.9 Torr for 3 min. The FIB milling was done in an FEI Helios Nanolab 660 using lift-out sample preparation technique. Structural analysis and elemental analysis with Energy Dispersive X-ray Spectroscopy (EDX) were performed in a Carl Zeiss Libra 200 Transmission Electron Microscope (TEM) operating at an accelerating voltage of 200 kV. Evaluation of the coating-to-substrate adhesion was carried out with the scratch-test method on the CSM Macro Scratch Tester Revetest with an indenter of 20 μm in radius. Maximum indentation load was 30 N. The scratch length was set to 7 mm. The images of the tracks were made with the optical microscope which is included as a standard module at 5× magnification. In order to obtain statistically meaningful data, each measurement was repeated at least three times per sample. To determine the molecular bonds in the Zn-HA coatings formed on Ti a research complex Centaur UHR (Nano Scan Technology, Russia) with a Raman spectrometer was used. Raman scattering was performed at room temperature with a laser excitation at the wavelength of $\lambda = 532.8$ nm and power of $P < 50$ mW.

RESULTS AND DISCUSSION

In **Figure 1A**, CP Ti substrate is represented by equiaxed coarse grains. The TEM inspection (**Figure 1B**) showed that the multiple uniaxial pressing allows the formation of a nanostructured state in the bulk Ti. After SPD, the size of the Ti grains is drastically decreased to an average of 85 ± 10 nm and represented by grains of elongated shape. The selected area diffraction (SAD) confirmed a high level of crystallinity and UFG state of Ti after SPD.

It is expected that the increased amount of dislocation and grain borders will increase the probability to form a crystalline HA-Zn coating. It is believed that surface defects and grain borders could act as points of nucleation when adatoms condense on the substrate from magnetron discharge plasma.

In **Figure 2**, an overview of the thin lamella of HA-Zn on UFG Ti placed on the Cu sample holder is shown. A set of the layers are represented in this figure, where HA-Zn is the coating deposited by RF magnetron sputtering, the Au/Pd coating was deposited to provide a conductive surface on the dielectric HA material and protective Pt layer is needed to protect the region of interest from ion milling. The thickness of the HA-Zn coating was determined as 458 ± 20 nm (**Figure 2B**), which corresponds to the thickness estimated by Calotest measurement.

The thickness of the coatings is well determined by two methods. From this, we recalculate the deposition rate in our magnetron sputtering system which is equal to 2.5 nm/min. In contrast, average coating growth rate reported by other research group for HA films is around 1 nm/min and less when the target-to-substrate distance was set to 40 mm (Ivanova et al., 2015). Hence, we conclude that the deposition rate in our sputtering system could be considered as high, which will affect the growing coating.

The TEM images of the coating are presented in **Figure 3**. On top of the HA coating, a protective Pt layer deposited during FIB sample preparation and a conductive Au/Pd layer deposited prior SEM are shown. From the **Figure 3B**, it is concluded that the HA-Zn coating has an equiaxed grain structure.

Interestingly, in our previous studies, deposited coating structure was represented by amorphous calcium phosphate. It is possible that the UFG structure of Ti substrate governed the growth of the coating which resulted in the equiaxed grain structure we observe in TEM micrographs. Note, that this type of structure is rarely produced in magnetron sputtering systems due to the hexagonal structure of the HA and the deposition process being non-equilibrium. A preliminary growth of columnar-like grain

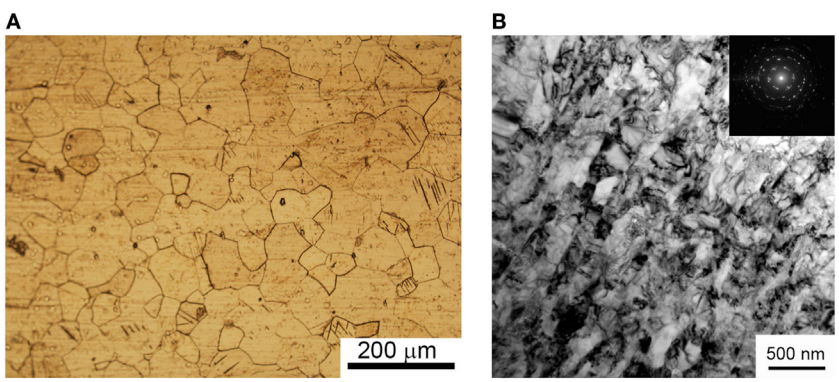

FIGURE 1 | Micrograph from optical metallography microscope of coarse grain commercially pure Ti **(A)** and TEM image of ultrafine-grained Ti after severe plastic deformation **(B)**.

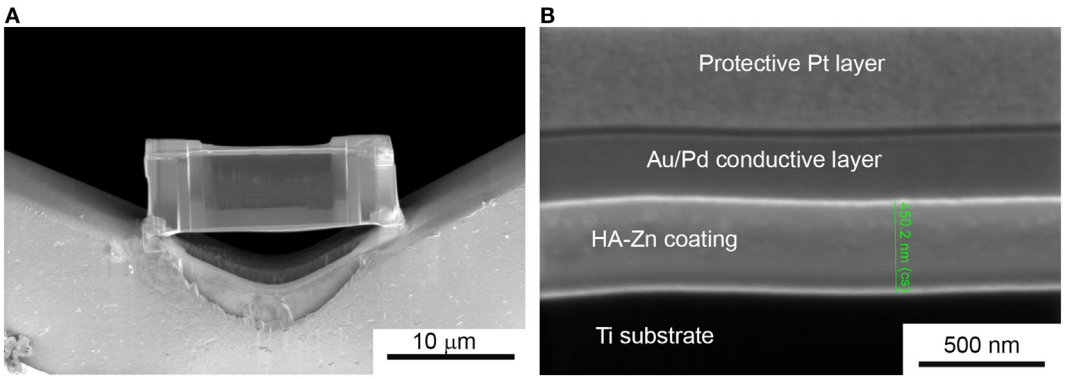

FIGURE 2 | Thin lamella of the Zn substituted HA coating deposited on ultrafine-grained Ti **(A)**, cross-section SEM shows a set of protective and conductive layers on the deposited film with an estimated HA-Zn coating thickness **(B)**.

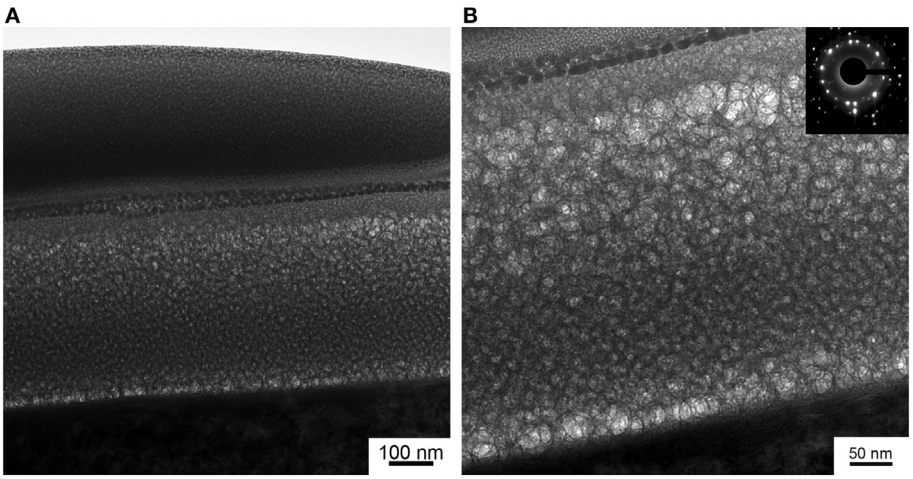

FIGURE 3 | Cross-section view on the gradient HA-Zn coating under conductive and protective layers **(A)** and the high magnification image of HA-Zn coating with a selected area diffraction micrograph **(B)**.

has been reported by other authors (Surmeneva et al., 2014). In **Figure 3B**, SAD micrograph gathered from the thin film region confirms the high crystallinity level of the deposited HA-Zn coating. The SAD proves the polycrystalline state of the coating. Interplanar *d*-spacings were calculated (2.39, 3.50, 4.07, 5.25 Å) and conform with a standard for HA (ICDD PDF No. 9-432). Moreover, it is possible to see that the coating is represented by the gradient type of structure, so that grain sizes are changing from the bottom to the top layer of the coating. It is worth to mention that the equiaxed grain structure has low residual inner stress compared to the columnar type of structure. Hence, this type of coating possibly will provide a higher level of stability to the coating in the case of mechanical stresses introduced during implantation surgery and service.

In **Figure 4**, a plot of the grain size gradient calculated from the micrograph of the interface between coating and substrate to

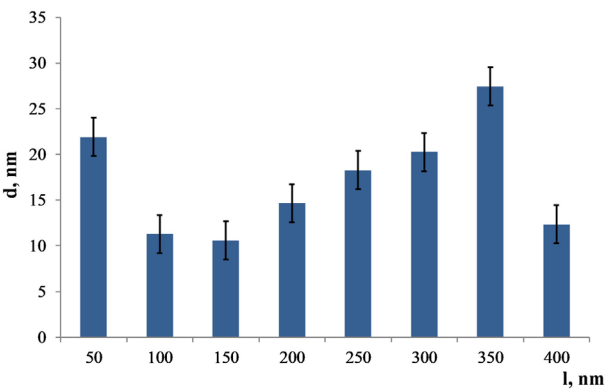

FIGURE 4 | Distribution of the Zn substituted HA grain sizes from the bottom to the top (l = 400 nm) layer of the coating.

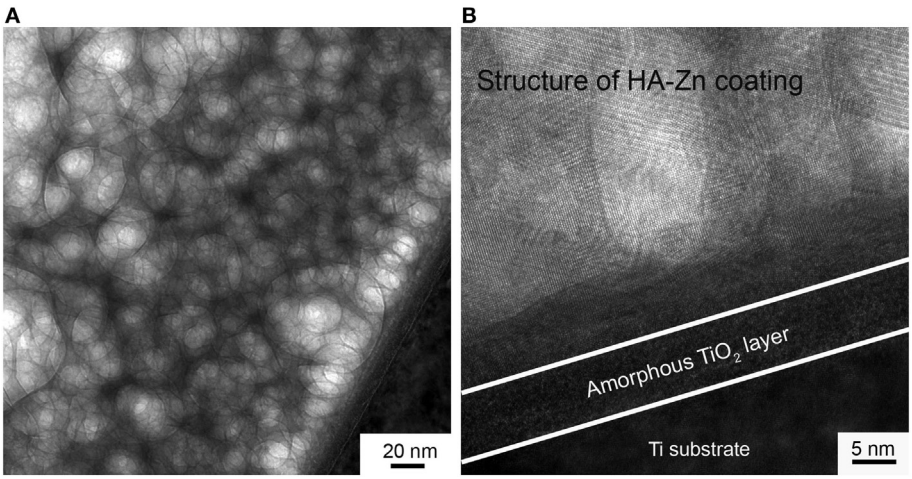

FIGURE 5 | The structure of deposited coating imaged in scanning TEM mode **(A)** and the micrograph of the coating to substrate interface with an amorphous sublayer **(B)**.

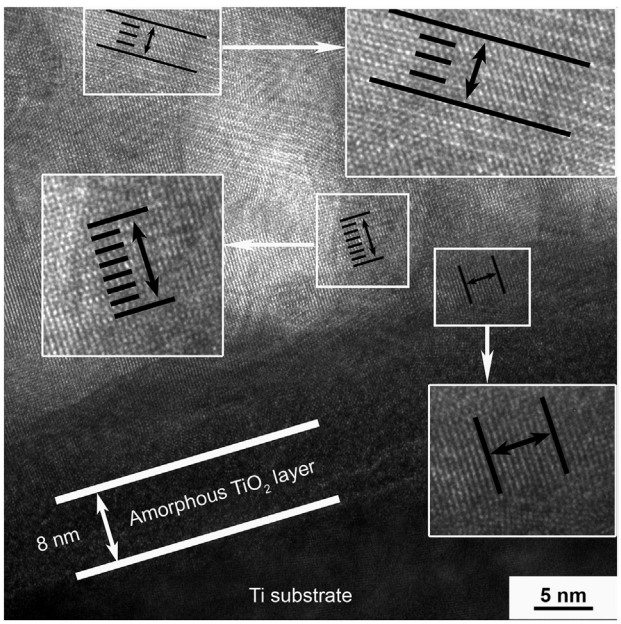

FIGURE 6 | Interplanar *d*-spacing measured in a fragment of high-resolution TEM of the HA-Zn coating.

the top layer is presented. The bimodal distribution depicts the significant scattering in the coating's grain size.

The largest grains are detected in the 350 nm distance from the substrate and equal to 27 ± 3 nm. However, grains start to grow from the amorphous layer reaching a diameter of 22 ± 3 nm. After that, grain sizes decrease dramatically at the distance of 150 nm from the substrate, reaching only 10 ± 3 nm. Thus, the coating morphology represents a complex gradient with a relatively large scattering of grain sizes. Note that the thin layer comprised of that type of structure is X-ray amorphous; therefore, it was not possible to get an X-ray diffraction pattern with HA peaks from those samples.

In **Figure 5**, TEM image obtained in the scanning mode is presented. Here, we see the overlapping grains of the coating. So the coating is represented by the complex misaligned structure. The high-resolution TEM (HRTEM) provided an opportunity to see atomic layers (**Figure 5B**). Moreover, an amorphous sublayer of 8 nm thickness at the interface between the substrate and the coating is detected. As it was reported in Surmeneva et al. (2014), the RF magnetron deposition process formed nano-scale grains, generating an amorphous layer of HA at the substrate/coating interface.

In our case, we detect amorphous layer at the interface between the crystalline coating and UFG Ti substrate which is constituted of TiO_2 according to EDX data. We associate this to the prior to deposition etching of the UFG Ti with an ion source. During this process, the naturally occurring TiO_2 layer was removed from the Ti surface. Subsequently, when an oxygen-containing sputtered species such as CaO or PO_4 reached the Ti surface, it could lead to a more energetically favorable occurring TiO_2 layer. On the other hand, high deposition rate and low substrate temperature prohibited the formation of crystalline structure. Then, at a certain thickness of the amorphous TiO_2 layer and due to the thermal conditions and surface free energy change, a crystalline structure of HA-Zn started to grow. Those conclusions are supported by the report of the scientific group (Göncü et al., 2017) dealing with HA-hexagonal boron nitride deposition on Ti.

Interplanar *d*-spacing measured in a fragment of HRTEM (**Figure 6**) correspond to peaks in the SAD pattern and results in 2.32, 4.1, 5.17 Å. Even though there are small deviations in estimated and standard numbers for HA which is attributed to overlapping grain structure and plausible inclination of a lamella during observation. The above-mentioned results correspond to the (122), (200), and (101) lattice planes for hexagonal HA.

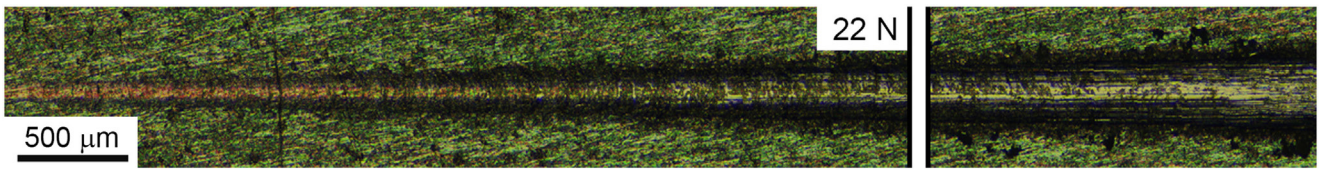

FIGURE 7 | Optical image of the indentation track with a load starting from 0.5 to 30 N on the HA-Zn coating deposited on ultrafine-grained Ti.

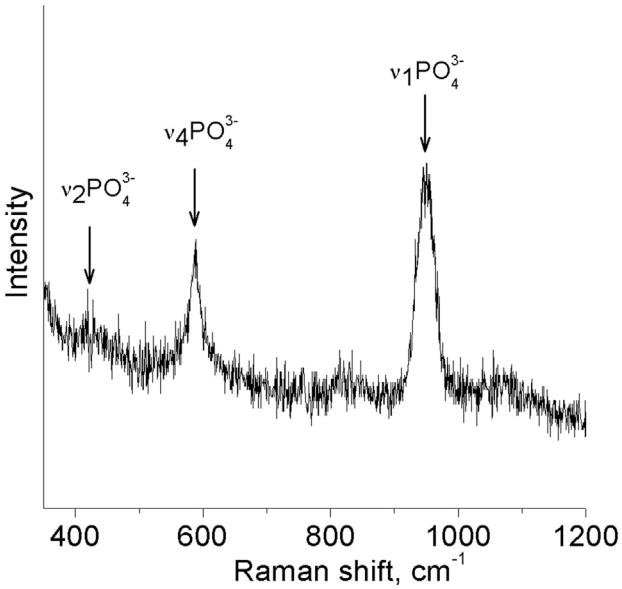

FIGURE 8 | Raman spectra gathered from the surface of HA-Zn coating.

Therefore, we could confirm that there is no separate phase of Zn and the obtained coating has the structure of the HA, even though Ca to Zn substitution took place. The EDX data gathered from the region shown in **Figure 6** present a typical pattern for HA coating. The Ca/P ratio of the deposited coating is 1.4 which corresponds to sub-stoichiometric HA. It is reported (Dorozhkin, 2012) that, with a decrease in Ca/P ratio, HA becomes more bioresorbable. That is beneficial for our coating because it will provide dissolution and release of the antibacterial Zn ions in the vicinity of the implantation site diminishing the bacterial colonization. However, according to the EDX data, Zn is represented by the small peak slightly higher than the noise level. This is due to the low concentration of Ca substitution in the coatings' material. Further antimicrobial and cytotoxicity tests are needed in order to confirm an effect of Zn incorporation into HA structure.

In **Figure 7**, the result of an HA-Zn scratching test is shown. From it, we see that significant coating tear off has started from the 22 N load. Due to the small thickness of the coating, there is no significant delamination seen, rather than spread and fade of the thin film under the load in the manner that regions near to the damaged site are not affected.

This effect may be useful for a coating deposited on intramedullary fixators that suffer severe damage during the implantation. Our coating provides high-level adhesion to the substrate and can tolerate mechanical stresses below 20 N without significant damage.

For investigation of chemical bonds in the coating and detection of characteristic HA structure peaks, Raman spectroscopy was utilized. The strongest Raman active ν_1 PO_4 mode (**Figure 8**) appears in the spectrum of the HA sample at 963/cm (Markovic et al., 2004).

It is seen that there are no shifts in spectra, and the majority of PO_4 vibration modes are easily distinguishable. That could be associated with the high level of crystallinity of the HA-Zn coating even though grain sizes do not exceede 30 nm (Antonakos et al., 2007). Despite that, Raman spectroscopy confirmed the presence of the P–O bond in the main intensity region for HA.

CONCLUSION

The HA-Zn was deposited on a technically pure UFG Ti substrate using the RF magnetron sputtering method. The FIB-prepared lamellas of the bioactive HA-Zn coating were studied using SEM, TEM, and EDX. The TEM results confirmed the gradient structure of the coating comprised of unoriented and overlapping equiaxed grains. The presence of an equiaxed grain structure with lattice plane orientations corresponding to (122), (200), and (101) of HA was observed. An amorphous TiO_2 sublayer of 8 nm thickness was detected in the interface between the polycrystalline coating and the UFG Ti substrate which contributes to the high coating to substrate adhesion level confirmed by a scratch test. The coatings chemical bonds investigation with a Raman spectroscopy method confirmed the presence of phosphate groups. The ratio of Ca/P equals to 1.4, which is indicated as the sub-stoichiometric HA. The possible antibacterial effect of Zn ions, high level of crystallinity, good adhesion to the substrate, and decreased Ca/P ratio could be a good candidate for a coating on intramedullary fixators in the presence of osteomyelitis or other bone infection.

AUTHOR CONTRIBUTIONS

KP, YS, and OB contributed conception and design of the study; OB provided assistance in the target sintering, KP prepared the samples, and UM performed high-resolution TEM imaging and provided his experience in the results description; KP wrote the first draft of the manuscript; KP, YS, OB, and UM contributed to the sections of the manuscript and participated in the fruitful

discussion of the results. All authors contributed to manuscript revision, read, and approved the submitted version.

ACKNOWLEDGMENTS

The authors thank Yu. Glushko for his support of the research. The authors also would like to thank Prof. M. Chaikina from the Institute of Mechanochemistry, Novosibirsk, Russia for synthesizing the HA-Zn powder. Y. Standke, Fraunhofer Institute for Ceramic Technologies and Systems Dresden, Germany, and A. Tahn, Technical University Dresden, Germany, provided their experience for FIB sample preparation. The authors are thankful to Prof. Dr. E. Zschech Fraunhofer Institute for Ceramic Technologies and Systems Dresden, Germany for valuable comments and fruitful discussion of the results.

FUNDING

The study was conducted as part of the program of fundamental research of Russian Academy of Science for 2018–2020, No. 23.2.5.

REFERENCES

Albrektsson, T., Canullo, L., Cochran, D., and De Bruyn, H. (2016). "Peri-implantitis": a complication of a foreign body or a man-made "disease" facts and fiction. *Clin. Implant Dent. Relat. Res.* 18, 840–849. doi:10.1111/cid.12427

Antonakos, A., Liarokapis, E., and Leventouri, T. (2007). Micro-Raman and FTIR studies of synthetic and natural apatites. *Biomaterials* 28, 3043–3054. doi:10.1016/j.biomaterials.2007.02.028

Asri, R. I. M., Harun, W. S. W., Hassan, M. A., Ghani, S. A. C., and Buyong, Z. (2016). A review of hydroxyapatite-based coating techniques: sol-gel and electrochemical depositions on biocompatible metals. *J. Mech. Behav. Biomed. Mater.* 57, 95–108. doi:10.1016/j.jmbbm.2015.11.031

Bartold, P. M., Ivanovski, S., and Darby, I. (2016). Implants for the aged patient: biological, clinical and sociological considerations. *Periodontol* 2000, 120–134. doi:10.1111/prd.12133

Chung, R. J., Hsieh, M. F., Huang, C. W., Perng, L. H., Wen, H. W., and Chin, T. S. (2006). Antimicrobial effects and human gingival biocompatibility of hydroxyapatite sol-gel coatings. *J. Biomed. Mater. Res. Part B Appl. Biomater.* 76, 169–178. doi:10.1002/jbm.b.30365

Dorozhkin, S. V. (2012). Amorphous calcium orthophosphates: nature, chemistry and biomedical applications. *Int. J. Mater. Chem.* 2, 19–46. doi:10.5923/j.ijmc.20120201.04

George, D. A., Gil, E., and Morris-Jones, S. (2016). "Prevention of periprosthetic joint infections: minimizing the risks," in Daniel, K., Rhidian, M-J., and Fares S. H., editors. *Periprosthetic Joint Infections: Changing Paradigms*. Springer International Publishing, 29–43.

Göncü, Y., Geçgin, M., Bakan, F., and Ay, N. (2017). Electrophoretic deposition of hydroxyapatite-hexagonal boron nitride composite coatings on Ti substrate. *Mater. Sci. Eng. C* 79, 343–353. doi:10.1016/j.msec.2017.05.023

Graziani, V., Fosca, M., Egorov, A. A., Zobkov, Y. V., Fedotov, A. Y., Baranchikov, A. E., et al. (2016). Zinc-releasing calcium phosphate cements for bone substitute materials. *Ceram. Int.* 42, 17310–17316. doi:10.1016/j.ceramint.2016.08.027

Gross, K. A., Saber-Samandari, S., and Heemann, K. S. (2010). Evaluation of commercial implants with nanoindentation defines future development needs for hydroxyapatite coatings. *J. Biomed. Mater. Res. Part B Appl. Biomater.* 93, 1–8. doi:10.1002/jbm.b.31537

Ivanova, A. A., Surmeneva, M. A., Surmenev, R. A., and Depla, D. (2015). Influence of deposition conditions on the composition, texture and microstructure of RF-magnetron sputter-deposited hydroxyapatite thin films. *Thin Solid Films* 591, 368–374. doi:10.1016/j.tsf.2015.03.058

Koo, H., Allan, R. N., Howlin, R. P., Stoodley, P., and Hall-Stoodley, L. (2017). Targeting microbial biofilms: current and prospective therapeutic strategies. *Nat. Rev. Microbiol.* 15, 740–755. doi:10.1038/nrmicro.2017.99

Li, X., Sogo, Y., Ito, A., Mutsuzaki, H., Ochiai, N., Kobayashi, T., et al. (2009). The optimum zinc content in set calcium phosphate cement for promoting bone formation in vivo. *Mater. Sci. Eng. C* 29, 969–975. doi:10.1016/j.msec.2008.08.021

Markovic, M., Fowler, B., and Tung, M. (2004). Preparation and comprehensive characterization of a calcium hydroxyapatite reference material. *J. Res. Natl.* 109, 553–568. doi:10.1016/j.ijpharm.2011.05.078

Mora-Sanchez, H., Sabirov, I., Monclus, M. A., Matykina, E., and Molina-Aldareguia, J. M. (2016). Ultra-fine grained pure titanium for biomedical applications. *Mater. Technol.* 31, 756–771. doi:10.1080/10667857.2016.1238131

Pacelli, S., Manoharan, V., Desalvo, A., Lomis, N., Jodha, K. S., Prakash, S., et al. (2016). Tailoring biomaterial surface properties to modulate host-implant interactions: implication in cardiovascular and bone therapy. *J. Mater. Chem. B* 4, 1586–1599. doi:10.1039/C5TB01686J

Podaropoulos, L., Veis, A. A., Trisi, P., Papadimitriou, S., Alexandridis, C., and Kalyvas, D. (2016). Bone reactions around dental implants subjected to progressive static load: an experimental study in dogs. *Clin. Oral Implants Res.* 27, 910–917. doi:10.1111/clr.12658

Prosolov, K. A., Popova, K. S., Belyavskaya, O. A., Rau, J. V., Gross, K. A., Ubelis, A., et al. (2017). RF magnetron-sputtered coatings deposited from biphasic calcium phosphate targets for biomedical implant applications. *Bioact. Mater.* 2, 170–176. doi:10.1016/j.bioactmat.2017.07.003

Rau, J. V., Cacciotti, I., Laureti, S., Fosca, M., Varvaro, G., and Latini, A. (2015). Bioactive, nanostructured Si-substituted hydroxyapatite coatings on titanium prepared by pulsed laser deposition. *J. Biomed. Mater. Res. Part B Appl. Biomater.* 103, 1621–1631. doi:10.1002/jbm.b.33344

Robinson, L., Salma-Ancane, K., Stipniece, L., Meenan, B. J., and Boyd, A. R. (2017). The deposition of strontium and zinc co-substituted hydroxyapatite coatings. *J. Mater. Sci. Mater. Med.* 28, 51. doi:10.1007/s10856-017-5846-2

Sedelnikova, M. B., Sharkeev, Y. P., Komarova, E. G., Khlusov, I. A., and Chebodaeva, V. V. (2016). Structure and properties of the wollastonite calcium phosphate coatings deposited on titanium and titanium niobium alloy using microarc oxidation method. *Surf. Coatings Technol.* 307, 1274–1283. doi:10.1016/j.surfcoat.2016.08.062

Sharkeev, Y., Komarova, E., Sedelnikova, M., Sun, Z. m., Zhu, Q. f., Zhang, J., et al. (2017). Structure and properties of micro-arc calcium phosphate coatings on pure titanium and Ti–40Nb alloy. *Trans. Nonferrous Met. Soc. China* 27, 125–133. doi:10.1016/S1003-6326(17)60014-1

Sharkeev, Y. P., Eroshenko, A. Y., Kovalevskaya, Z. G., Saprykin, A. A., Ibragimov, E. A., Glukhov, I. A., et al. (2016). Structural and phase state of Ti–Nb alloy at selective laser melting of the composite powder. *Russ. Phys. J.* 59, 430–434. doi:10.1007/s11182-016-0790-z

Sharkeev, Y. P., Legostaeva, E. V., Eroshenko, Y. A., Khlusov, I. A., and Kashin, O. A. (2009). The structure and physical and mechanical properties of a novel biocomposite material, nanostructured titanium–calcium-phosphate coating. *Compos. Interfaces* 16, 535–546. doi:10.1163/156855409X447174

Sidambe, A. T. (2014). Biocompatibility of advanced manufactured titanium implants – a review. *Materials (Basel)* 7, 8168–8188. doi:10.3390/ma7128168

Šupová, M. (2015). Substituted hydroxyapatites for biomedical applications: a review. *Ceram. Int.* 41, 9203–9231. doi:10.1016/j.ceramint.2015.03.316

Surmeneva, M. A., Surmenev, R. A., Nikonova, Y. A., Selezneva, I. I., Ivanova, A. A., Putlyaev, V. I., et al. (2014). Fabrication, ultra-structure characterization and in vitro studies of RF magnetron sputter deposited nano-hydroxyapatite thin films for biomedical applications. *Appl. Surf. Sci.* 317, 172–180. doi:10.1016/j.apsusc.2014.08.104

Toth, L. S., and Gu, C. (2014). Ultrafine-grain metals by severe plastic deformation. *Mater. Charact.* 92, 1–14. doi:10.1016/j.matchar.2014.02.003

Valiev, R. Z., Estrin, Y., Horita, Z., Langdon, T. G., Zehetbauer, M. J., and Zhu, Y. (2016). Producing bulk ultrafine-grained materials by severe plastic deformation: ten years later. *JOM* 68, 1216–1226. doi:10.1007/s11837-016-1820-6

Vladescu, A., Surmeneva, M. A., Cotrut, C. M., Surmenev, R. A., and Antoniac, I. V., editors. (2016). "Bioceramic coatings for metallic implants," in *Handbook of Bioceramics and Biocomposites*. Springer International Publishing, 703–733.

Wen, H. B., De Wijn, J. R., Cui, F. Z., and De Groot, K. (1998). Preparation of calcium phosphate coatings on titanium implant materials by simple chemistry. *J. Biomed. Mater. Res.* 41, 227–236. doi:10.1002/(SICI)1097-4636(199808)41:2<227::AID-JBM7>3.0.CO;2-K

Conflict of Interest Statement: The authors declare that the research was conducted in the absence of any commercial or financial relationships that could be construed as a potential conflict of interest.